

Article

Effects of *n*-Butanol Addition on the Combustion Characteristics of *n*-Heptane Counterflow Diffusion Flame at Elevated Pressure

Yaoyao Ying ^{1,2,*}  and Dong Liu ^{1,2,*} 

¹ MITT Key Laboratory of Thermal Control of Electronic Equipment, School of Energy and Power Engineering, Nanjing University of Science and Technology, Nanjing 210094, China

² Advanced Combustion Laboratory, School of Energy and Power Engineering, Nanjing University of Science and Technology, Nanjing 210094, China

* Correspondence: yingyaoyao@njjust.edu.cn (Y.Y.); dongliu@njjust.edu.cn (D.L.)

Abstract: This study focused on the effects of *n*-butanol addition on the combustion characteristics of *n*-heptane counterflow diffusion flame under pressures of 1, 3, and 5 atm by a detailed kinetic simulation. The added *n*-butanol volume fraction ranged from 0 to 50%. The mass averaged velocity of fuel streams was selected to ensure momentum flux balance and was approximately constant for the investigated flames. Flame structures and mole fraction profiles impacted by *n*-butanol addition for major species, free radicals, and intermediate species were analyzed by concentrating on the formations of soot precursors and oxygenated air pollutants. The results showed that with the addition of *n*-butanol, the flame temperature decreased and the formation of the main soot precursors such as C₂H₂ and C₆H₆ was inhibited. This can be attributed to the reduced rate of production of these species. The flame temperature increased significantly, and the profile moved towards the fuel side with the increasing pressure. Moreover, the production of C₂H₂ and C₆H₆ was observably promoted as the pressure increased. The concentrations of free radical H, O, and OH decreased significantly as the pressure increased but slightly decreased with the increasing *n*-butanol addition, which might have been caused by the chemical effect of *n*-butanol.

Keywords: counterflow diffusion flame; *n*-heptane; *n*-butanol addition; chemical kinetics



Citation: Ying, Y.; Liu, D. Effects of *n*-Butanol Addition on the Combustion Characteristics of *n*-Heptane Counterflow Diffusion Flame at Elevated Pressure. *Fire* **2022**, *5*, 154. <https://doi.org/10.3390/fire5050154>

Academic Editors: Xuehui Wang and Qinpei Chen

Received: 4 September 2022

Accepted: 29 September 2022

Published: 30 September 2022

Publisher's Note: MDPI stays neutral with regard to jurisdictional claims in published maps and institutional affiliations.



Copyright: © 2022 by the authors. Licensee MDPI, Basel, Switzerland. This article is an open access article distributed under the terms and conditions of the Creative Commons Attribution (CC BY) license (<https://creativecommons.org/licenses/by/4.0/>).

1. Introduction

Energy plays an important role in the development and progress of human society. The development of science and technology promotes the improvement of the energy utilization level and scale, which continuously facilitates the growth of human society to a new stage. At present, the overall energy consumption of the world is still dominated by fossil fuels [1–3]. However, the utilization of fossil fuels also brings problems. The combustion of fossil fuels releases air pollutants and greenhouse gases, polluting the environment and contributing to global warming [4,5]. Moreover, the incomplete burning of fossil fuels generates soot, which is harmful to human health [6–8]. It is urgent and necessary to develop and use new renewable energy sources.

Biofuels, such as bio-ethanol, bio-butanol, and biodiesel, as alternatives to petroleum-based transportation fuels, have been of increasing interest in recent years due to the long-term promise of fuel-source renewability and climate-impact reduction [9]. Alcohols as oxygenated compounds stand out as good alternative fuels or fuel additives for the reduction of soot emissions and have been widely investigated [10–12]. Butanol is a very promising fuel alternative or additive that has higher energy density [13], lower water absorption, and better miscibility with present fuels, compared to ethanol [9].

Investigations of the effects of *n*-butanol on combustion fundamental characteristics have been extensively performed experimentally and numerically. Uyumaz [14] investi-

gated the combustion and performance characteristics of *n*-heptane, *n*-butanol, and isopropanol in an HCCI engine; the result showed that adding high octane number alcohols could extend the range of the HCCI operation and control autoignition. Liu et al. [15,16] also investigated to reveal the combustion characteristics and soot-reduction capability in HCCI combustion with different control strategies, and they found that the blends of gasoline and *n*-butanol in diesel significantly reduced soot emissions, and *n*-butanol addition presented a higher soot-reduction ability at a low diesel replacement ratio (30%). Wu et al. [17] simulated the combustion process in a diesel engine with *n*-butanol/diesel blends and found that the maximum combustion pressure and temperature increased and the accumulated heat of release reduced with *n*-butanol addition. Chen et al. [18] conducted an experimental study on the effects of the energy substitution ratio on the combustion characteristics and performance of a diesel engine fuelled with methanol, ethanol, and *n*-butanol addition, and the results showed that the alcohol additions decreased the particle concentration. The effect of *n*-butanol addition with isooctane and *n*-heptane on ignition delay times was obtained in a constant volume combustion chamber; it was presented that *n*-butanol addition inhibited the ignition delay time and reduced reactivity [19]. Zheng et al. [20] experimentally investigated the influence of two-stage injection on the combustion and emission characteristics in a single-cylinder diesel engine with pure diesel, and blended, fuels of gasoline and *n*-butanol, and the results showed that with the addition of gasoline and *n*-butanol, a slight increase in indicated thermal efficiency was induced and the smoke emissions were more sensitive to the change in post-injection strategy. An experimental study of combustion characteristics with *n*-heptane direct injection and *n*-butanol pipe injection in an HCCI engine was carried out by Zhang et al. [21], and they found that *n*-heptane direct injection could improve *n*-butanol combustion and reduce HC and CO emissions. Yu et al. [22] used *n*-butanol as a substituted fuel for spark ignition aviation piston engines to study the engine performance, and they found that the heat release of *n*-butanol was more concentrated and *n*-butanol could achieve higher brake thermal efficiency. The combustion and emission characteristics of *n*-heptane with three oxygenated fuels, including *n*-butanol, benzaldehyde, and anisole, were experimentally studied on a heavy-duty diesel engine, and the results showed that the *n*-butanol addition led to lower soot emissions and higher NO_x emissions with increasing injection pressure [23].

To our knowledge, the study of the detailed effects of *n*-butanol addition on the formations and consumptions of important species, including some soot precursors and oxygenated air pollutants at elevated pressure, is limited. This is the first time a comprehensive numerical study is being performed on a counterflow diffusion flame of *n*-butanol/*n*-heptane blended fuel for a thorough understanding of the flame chemistry at elevated pressure. The present study aims to explore the effects of *n*-butanol addition on *n*-heptane flames, with an emphasis on the pollutant species by kinetic analysis.

2. Kinetic Modeling and Analysis Method

The detailed chemical reaction mechanism for *n*-heptane and *n*-butanol combustion used here is POLIMI_BIOGASOLINE_171R developed by Ranzi et al. [24], which consists of 171 species and 3860 reactions. The reduced mechanism is derived by including *n*-butanol in the previous ternary mixture of *n*-heptane, iso-octane, and toluene. The accuracy of the mechanism has been proved by numerous works and studies [25–27]. The simulations performed in this work were conducted by OpenSMOKE/CounterFlow-Flame1D code [28].

The counterflow configuration considered in this numerical study mimics a counterflow burner designed by Advanced Combustion Laboratory in NJUST. Only a brief overview is provided here as a comprehensive description is available in Ref [29]. The upper nozzle and the lower nozzle are used for the fuel and the oxidizer stream, respectively. The separation distance between the nozzles is 8.0 mm. On the fuel side, *n*-heptane was replaced by *n*-butanol ranging from 10% to 50% in volume fraction. On the oxidizer side, 79% nitrogen and 21% oxygen were mixed as the oxidizer. The detailed flame conditions

were listed in Table 1. The boundary temperatures of the fuel and oxidizer nozzle were maintained at 570 K and 300 K, respectively. The simulated pressure was 1, 3, and 5 atm.

Table 1. The detailed flame conditions.

No.	Pressure (atm)	Fuel Side			V_f (cm/s)	Oxidizer Side V_{OX} (cm/s)
		Volume Fraction (%)				
		NC ₇ H ₁₆	N1C ₄ H ₉ OH	N ₂		
1		10	0		16.39	
2		9	1		16.51	
3	1	8	2		16.63	
4		6	4		16.89	
5		5	5		17.01	
6		10	0		16.39	
7		9	1		16.51	
8	3	8	2	90	16.63	20
9		6	4		16.89	
10		5	5		17.01	
11		10	0		16.39	
12		9	1		16.51	
13	5	8	2		16.63	
14		6	4		16.89	
15		5	5		17.01	

3. Results

The mole fraction profiles and rate of production of vital components are calculated for all the simulated flames. Only the profiles that are thought to be most relevant to fuel consumption and important pollutant formations are discussed in this paper. The simulation results show that the variations of the flame temperature and mole fraction profiles of these species present a uniform trend with the *n*-butanol addition at the same pressure, respectively. There is no mutation with the increasing *n*-butanol addition. Thus, to make the figures clearer to read, typical conditions are selected to show the changing tendency with 0%, 20%, and 50% *n*-butanol addition at each pressure. Moreover, the rate of production analysis for reactant *n*-heptane and *n*-butanol, and some essential intermediate species, including acetylene (C₂H₂) and benzene (C₆H₆), are shown.

3.1. Flame Temperature Profiles

The intensity of flame burning can be measured by measuring multiple indicators, such as the light intensity of the flame, the flame temperature distribution, the fuel consumption rate, and the product generation rate. The flame temperature distribution is one of the most intuitive and effective indicators to identify the flame burning intensity.

The flame temperatures are shown in Figure 1a, with 0%, 20%, and 50% *n*-butanol additive at pressures of 1, 3, and 5 atm, and the locally enlarged view of flame temperature is presented in Figure 1b. It can be seen that at constant pressure, the flame temperature gradually decreased with the increasing *n*-butanol addition. The peak temperature decreased the most, and the temperature distribution was slightly narrowed when *n*-butanol was added. However, with the increase in pressure, the peak value of the flame temperature increased significantly, and the temperature peak position moved to the fuel side. The distribution of the flame temperature was also narrowed, which indicated that the reaction zone was narrowed at elevated pressure.

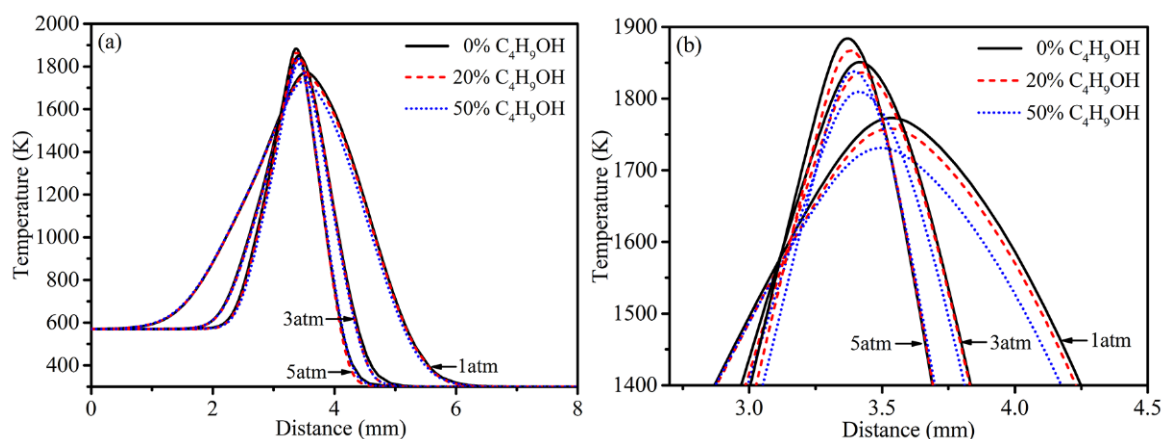


Figure 1. Temperature profiles of flame with different levels of *n*-butanol at different pressures: (a) total view, (b) locally enlarged view.

3.2. Major Species and Radicals

Figure 2 showed the mole fraction profiles of *n*-heptane with different levels of *n*-butanol addition at different pressures. The mole fraction of *n*-heptane decreased as the mole fraction of *n*-butanol increased since the total mole fraction of the mixed fuel was 10% on the fuel side (the other 90% was the diluted nitrogen) at the same pressure. However, the position where the *n*-heptane mole fraction decreased to zero was almost unchanged, which illustrated that the consumption of *n*-heptane was faster at higher *n*-heptane concentrations. The position of *n*-heptane started to react and moved to the oxidizer side when the pressure increased. At the same time, the slope of the mole fraction distribution became larger, indicating that the reaction rate of *n*-heptane increased with the increasing pressure. The position where the *n*-heptane was depleted was moving toward the oxidizer side slightly.

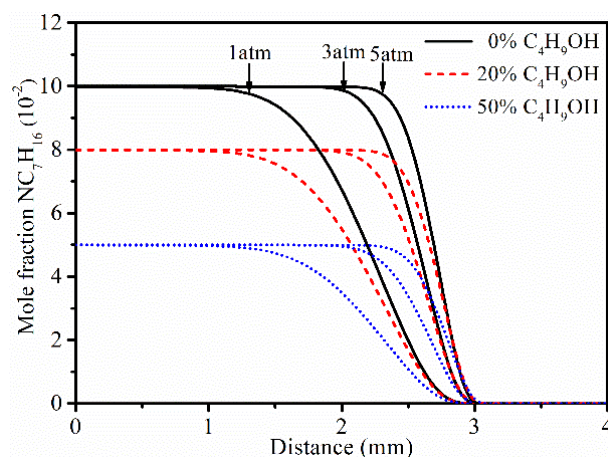


Figure 2. Mole fractions of NC₇H₁₆, with different levels of *n*-butanol at different pressures.

The rate of consumption of *n*-heptane with 0%, 20%, and 50% butanol addition was presented in Figure 3. The dominant consumption reactions of *n*-heptane were R742: $\text{NC}_7\text{H}_{16} = 0.2\text{CH}_3 + 0.4\text{C}_2\text{H}_5 + 0.4\text{NC}_3\text{H}_7 + 0.4\text{NC}_4\text{H}_9\text{P} + 0.5\text{NC}_5\text{H}_{11} + 0.1\text{NC}_7\text{H}_{15}$ and R2584: $\text{NC}_7\text{H}_{16} + \text{H} = \text{H}_2 + \text{NC}_7\text{H}_{15}$. Figure 3a,b shows the influence of R742 and R2584 on the consumption rate of *n*-heptane under different flame conditions. When the pressure was kept constant, the reaction rates of R742 and R2584 both decreased with the increasing addition of *n*-butanol. The position of the reaction rate curve hardly moved, which indicated that the consumption rate of *n*-heptane decreased due to the decrease in *n*-heptane concentration. The reaction rates of R742 and R2584 significantly increased with the increasing pressure.

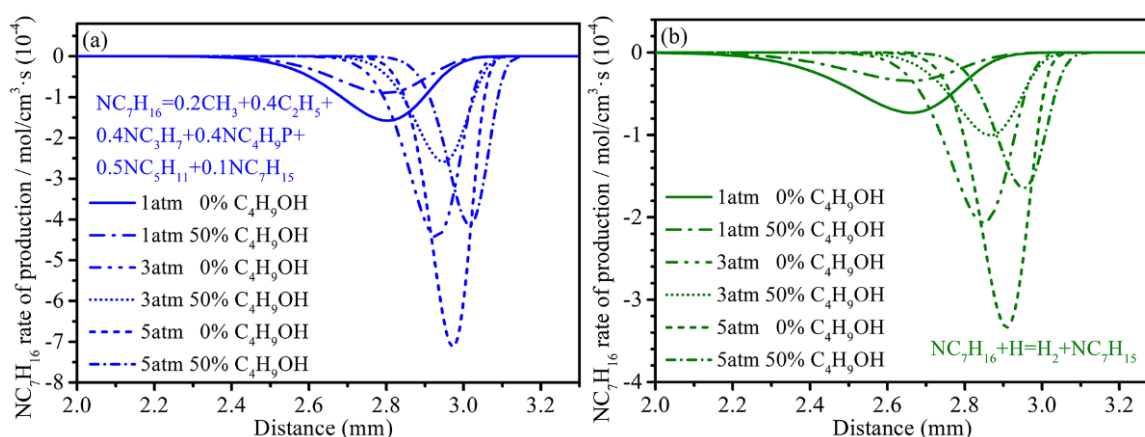


Figure 3. Rate of production of NC_7H_{16} , with different levels of *n*-butanol at different pressures. (a) 742, (b) R2584.

N-butanol was the fuel additive for this study. Figure 4 describes the distribution of the *n*-butanol mole fraction in different flame conditions. It was found that the position of the depletion of *n*-butanol was almost unchanged with the increasing *n*-butanol addition ratio, which can be attributed to the faster reaction rate of butanol in the reactions with higher mole fractions. When the pressure increased, the depleted point of *n*-butanol moved slightly toward the oxidizer side, and the slope of the mole fraction distribution curve increased, which revealed that *n*-butanol consumption was improved with higher pressure.

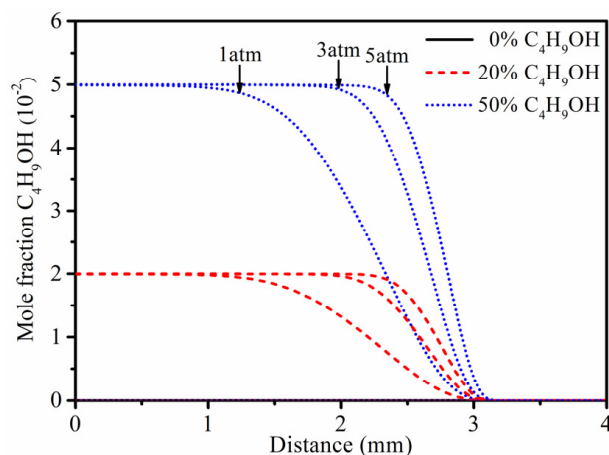


Figure 4. Mole fractions of $\text{C}_4\text{H}_9\text{OH}$, with different levels of *n*-butanol at different pressures.

Figure 5 gives the dominant consumption reactions of *n*-butanol at elevated pressures. The main reactions responsible for the consumption of *n*-butanol were R942: $\text{N1C}_4\text{H}_9\text{OH} = \text{H}_2\text{O} + \text{NC}_4\text{H}_8$, R936: $\text{N1C}_4\text{H}_9\text{OH} = \text{CH}_2\text{OH} + \text{NC}_3\text{H}_7$, and R3665: $\text{N1C}_4\text{H}_9\text{OH} + \text{H} = \text{H}_2 + \text{CH}_3\text{CH}_2\text{CH}_2\text{CHOH}$. The consumption rates of the three reactions all increased with the increased *n*-butanol addition at the same pressure. When the fuel composition remained unchanged, the consumption rate of *n*-butanol significantly increased as the pressure increased. Furthermore, the reaction rate curves moved to the oxidizer side at higher pressure conditions. The dramatic increase in the reaction rates of *n*-butanol consumption was a good explanation for the rapid decrease in *n*-butanol under high pressure, as shown in Figure 4.

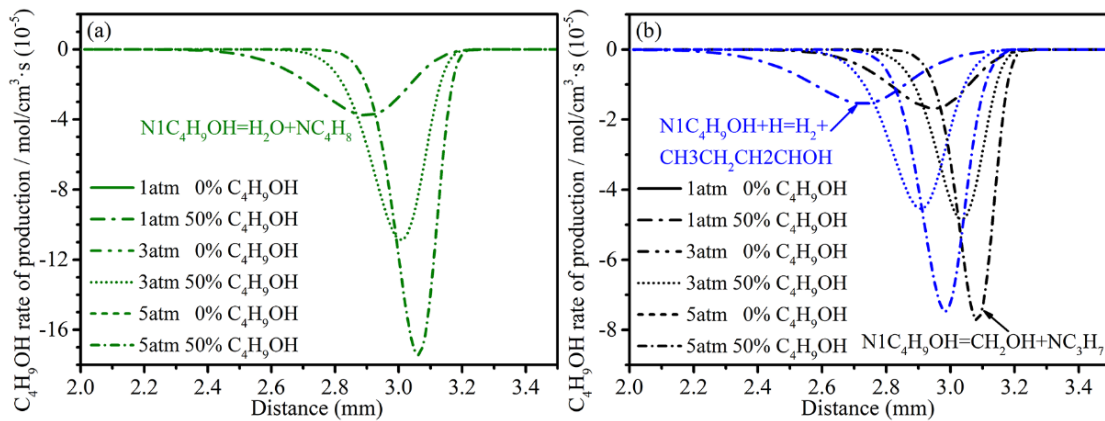


Figure 5. Rate of production of C_4H_9OH , with different levels of n -butanol at different pressures. (a) R942, (b) R936 and R3665.

From the view of the main reactions responsible for the consumption of n -heptane and n -butanol, the H radical played a vital role in the combustion. The mole fraction profile of H radical with different n -butanol fractions at elevated pressure is presented in Figure 6a. It can be seen that the peak mole fraction of the H radical decreased with the addition of n -butanol at constant pressure, and the peak position moved toward the fuel side. As the pressure increased, the peak value of H radical dropped sharply and the peak value position moved to the fuel side significantly. The peak value of the H radical at 5 atm reduced to about one-third of that at 1 atm. Moreover, the distribution curves were notably narrowed. The increased pressure inhibited the generation of H radicals.

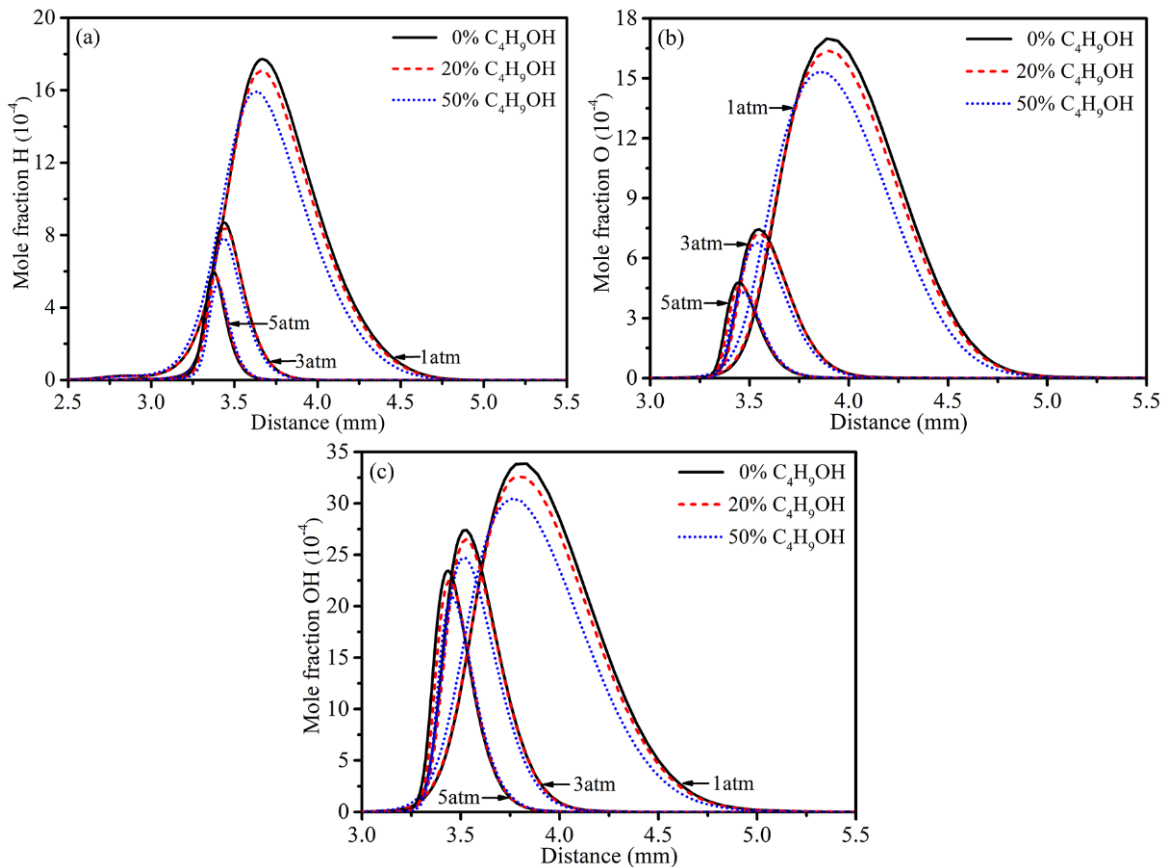


Figure 6. Mole fractions of (a) H radical, (b) O radical, and (c) OH radical, with different levels of n -butanol at different pressures.

The mole fraction profiles of O and OH radicals shown in Figure 6b,c exhibited similar variation trends to H radicals. The peak mole fractions of the O and OH radicals decreased with the increasing *n*-butanol addition under each pressure, which revealed that *n*-butanol addition inhibited the production of O and OH radicals. When the pressure increased, the peak concentrations of O and OH radicals reduced dramatically, and the narrowed peak position moved toward the fuel side. The pressure showed an inhibition effect on these three radicals, and it was more obvious in reducing the H and O radicals.

The mole fraction profiles of CO and CO₂ with different levels of *n*-butanol additives are presented in Figure 7a,b. CO and CO₂ concentrations decreased with the replacement of *n*-heptane by *n*-butanol at the same pressure. This illustrated that the *n*-butanol could slightly inhibit the formation of CO and CO₂, and the higher the ratio of *n*-butanol addition, the more obvious the inhibition effect, while with the same volume addition of *n*-butanol, the peak mole fraction values of CO decreased drastically when the pressure increased. On the contrary, the peak values of CO₂ concentrations increased with the increasing pressure, and the peak values positions moved toward the fuel side. This indicated that more carbon element was converted to CO₂ rather than CO. Furthermore, the distribution of the peak value of CO₂ kept the same variations as that of the fuels *n*-heptane and *n*-butanol corresponding to the former analysis.

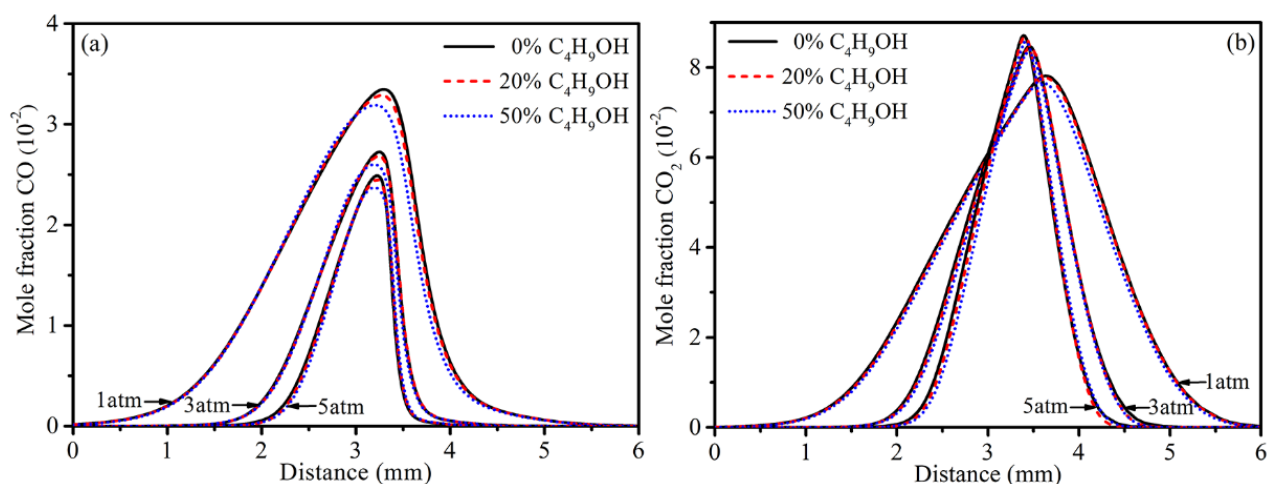


Figure 7. Mole fractions of (a) CO, and (b) CO₂ with different levels of *n*-butanol at different pressures.

3.3. Intermediate Species

As acetylene (C₂H₂) and benzene (C₆H₆) are important soot precursors, and formaldehyde and acetaldehyde are typical and harmful oxygenated air pollutants, they are discussed in detail.

Figures 8 and 9 show the mole fraction distributions of C₂H₂ and C₆H₆ with different levels of *n*-butanol additives at elevated pressures. It can be seen that the variation trends of C₂H₂ and C₆H₆ were consistent. When the pressure was constant, the concentrations of C₂H₂ and C₆H₆ significantly decreased with the increasing *n*-butanol additives, which illustrated that *n*-butanol addition could inhibit the formation of soot precursors. Westbrook et al. [30] concluded that nearly all of the oxygen atoms initially present in the oxygenate react directly to generate CO through a detailed chemical kinetic modeling investigation. As a result, the reduction in the two soot precursors can be attributed to the existence of the O element in *n*-butanol and oxidized more carbon elements to CO rather than C₂H₂ and C₆H₆.

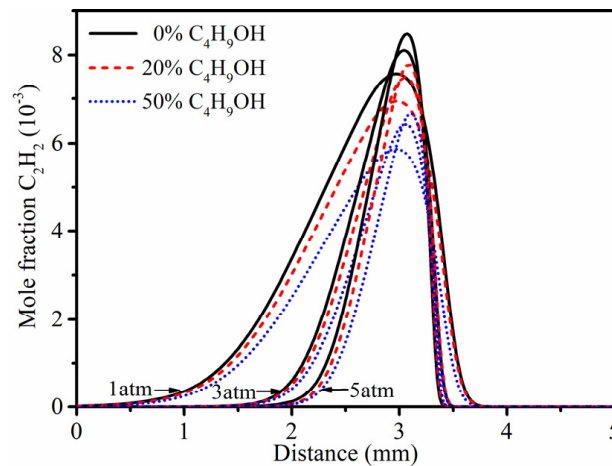


Figure 8. Mole fractions of C_2H_2 with different levels of n -butanol at different pressures.

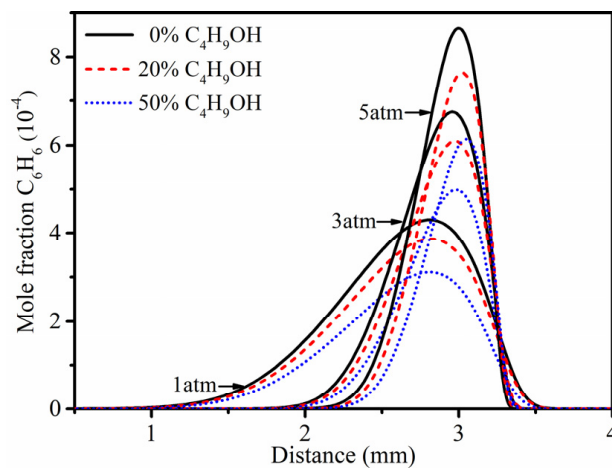


Figure 9. Mole fractions of C_6H_6 , with different levels of n -butanol at different pressures.

On the contrary, with the increase in pressure, the concentrations of C_2H_2 and C_6H_6 increased, and the distributions moved toward the oxidizer side. The peaks of the C_2H_2 distribution curve increased to a small degree and were not sensitive to pressure changes. The peak value of benzene at 5 atm was about twice that at 1 atm, and the increase was very obvious. The production areas of C_2H_2 and C_6H_6 were narrowed with increasing pressures. The total mole fractions of C_2H_2 and C_6H_6 were enhanced by the increased pressures.

The rates of production of C_2H_2 with 0%, 20%, and 50% n -butanol additions were given in Figure 10. The main formation reaction of acetylene was R82: $C_2H_3 (+M) = C_2H_2 + H (+M)$, and the main consumption reaction was R323: $C_2H_2 + O = H + HCCO$. It showed that with the increasing n -butanol additive, the reaction rates of the production and consumption reactions all decreased. The overall effects of n -butanol addition resulted in a decrease in C_2H_2 , as shown in Figure 8. When the fuel composition was kept constant, the reaction rates of R82 and R323 both increased with the increased pressure, and the reaction areas were narrowed. The combined effect promoted the generation of C_2H_2 . As pointed out by the well-known hydrogen abstraction carbon addition (HACA) mechanism [31], C_2H_2 is a key species that contributes to the growth of poly-aromatic hydrocarbon (PAH). Subsequently, it might result in higher soot formation with increasing pressure.

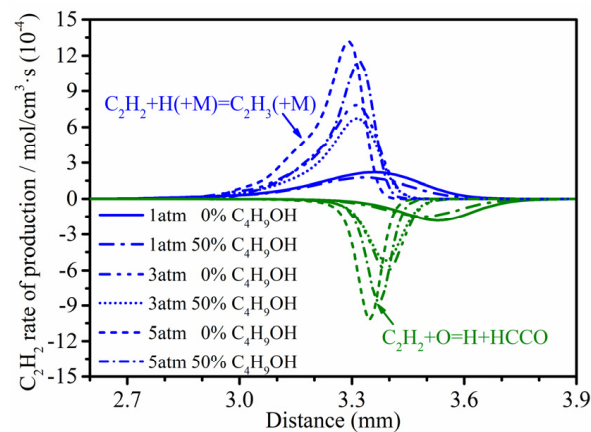


Figure 10. Rate of production of C_2H_2 , with different levels of n -butanol at different pressures.

Figure 11 presents the rate of production of C_6H_6 with different levels of n -butanol at different pressures. The main reactions responsible for C_6H_6 formations were R415: $C_6H_5 + H = C_6H_6$, and R419: $2C_3H_3 (+M) = C_6H_6 (+M)$. The dominant reaction for C_6H_6 consumption was R444: $C_6H_6 + H = H_2 + C_6H_5$. The formation and consumption reactions of C_6H_6 all decreased with increased n -butanol additives at constant pressure. The total C_6H_6 concentration was reduced as n -heptane was replaced by n -butanol. When the pressure increased, the formation and consumption reactions of C_6H_6 all increased and the final C_6H_6 concentration increased, as shown in Figure 9. By blending n -butanol into n -heptane, the oxygenated fuel increased oxygen atoms, which could effectively reduce the formation of soot precursors [32].

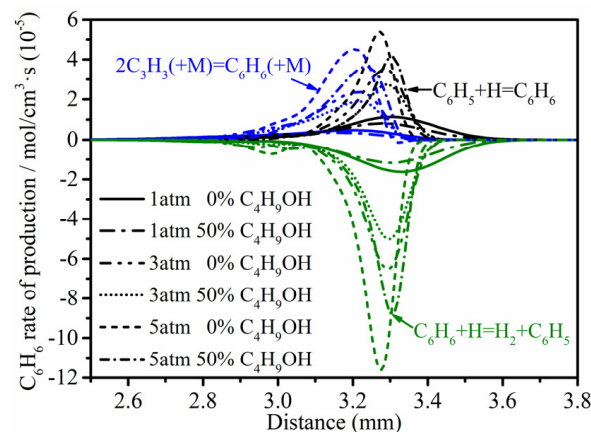


Figure 11. Rate of production of C_6H_6 , with different levels of n -butanol at different pressures.

Figures 12 and 13 present the concentrations of CH_2O and CH_3CHO in different flame conditions. The mole fractions of CH_2O and CH_3CHO increased significantly with the addition of n -butanol. The simulation results indicated an enhancement effect for increasing n -butanol in the reaction mixture. This was because the addition of n -butanol increased the oxygen content on the fuel side, which promoted the formation of oxygen-containing pollutants [33]. The mole fraction of CH_2O decreased as the pressure increased, and the position of the peak value of CH_2O moved toward the oxidizer side. While the peak concentration of CH_3CHO nearly kept the same at different pressures, the position of the peak value of CH_3CHO moved to the oxidizer side as well.

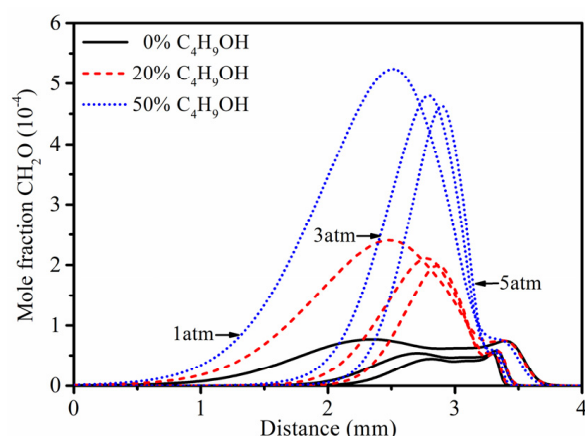


Figure 12. Mole fractions of CH_2O , with different levels of n -butanol at different pressures.

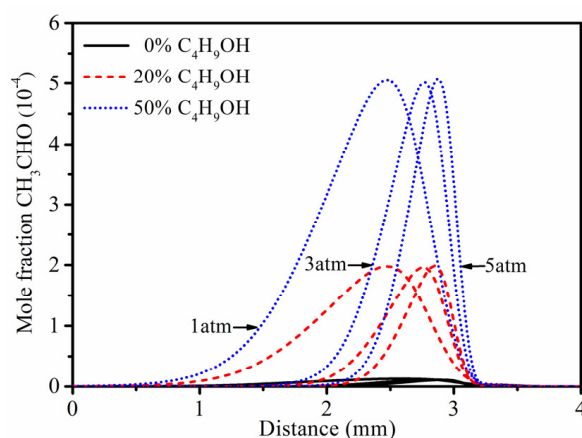


Figure 13. Mole fractions of CH_3CHO , with different levels of n -butanol at different pressures.

4. Conclusions

This study investigated the effects of n -butanol addition on the combustion characteristics of n -heptane counterflow diffusion flame under pressures of 1, 3, and 5 atm. The flame temperature and major species of reactants, soot precursors, and oxygenated air pollutants variations were analyzed. The results can be summarized as follows:

1. The flame temperature decreased with the addition of n -butanol, while the temperature increased with increasing pressures.
2. The addition of n -butanol inhibited the formation of CO , C_2H_2 , and C_6H_6 but promoted the formation of CO_2 , CH_2O , and CH_3CHO . This can be attributed to the increased oxygen content on the fuel side; thus, the oxygen-containing species increased.
3. The H , O , and OH radicals slightly decreased with n -butanol addition, while they dramatically reduced under higher pressures, especially the H and O radicals.
4. The increased pressure significantly enhanced the rates of the main production and consumption reactions and promoted total combustion.

Author Contributions: Conceptualization, methodology, validation, formal analysis, investigation, data curation, writing—original draft preparation, writing—review and editing, and visualization, Y.Y.; supervision, project administration, D.L.; and funding acquisition, Y.Y. and D.L. All authors have read and agreed to the published version of the manuscript.

Funding: This research was funded by Jiangsu Provincial Natural Science Foundation of China (BK20200490), the National Natural Science Foundation of China (52106160, 52076110), the Fundamental Research Funds for the Central Universities (30920031103), and the State Key Laboratory of Engines, Tianjin University.

Institutional Review Board Statement: Not applicable.

Informed Consent Statement: Not applicable.

Data Availability Statement: Not applicable.

Acknowledgments: The authors thank the support from the State Key Laboratory of Engines at Tianjin University.

Conflicts of Interest: The authors declare no conflict of interest.

References

1. Ryu, K. The characteristics of performance and exhaust emissions of a diesel engine using a biodiesel with antioxidants. *Bioresour. Technol.* **2010**, *101*, S78–S82. [[CrossRef](#)] [[PubMed](#)]
2. Gang, L.; Zhang, C.; Li, Y. Effects of diesel injection parameters on the rapid combustion and emissions of an HD common-rail diesel engine fueled with diesel-methanol dual-fuel. *Appl. Therm. Eng.* **2016**, *108*, 1214–1225.
3. Xie, H.; Yu, Y.; Wang, W.; Liu, Y. The substitutability of non-fossil energy, potential carbon emission reduction and energy shadow prices in china. *Energy Policy* **2017**, *107*, 63–71. [[CrossRef](#)]
4. Pauchard, J.-C.; Gress, G.; Biais, M.; Beloeil, H.; Nouette-Gaulain, K. Reducing the greenhouse gas emissions from halogenated agents in daily clinical practice: An audit at the University Hospital of Bordeaux. *Anaesth. Crit. Care. Pa.* **2020**, *39*, 685–687. [[CrossRef](#)]
5. Arienzo, M.M.; Maezumi, S.Y.; Chellman, N.J.; Iriarte, J. Pre-Columbian Fire Management Linked to Refractory Black Carbon Emissions in the Amazon. *Fire* **2019**, *2*, 31. [[CrossRef](#)]
6. Wang, Q.; Wu, Z. Effect of secondary air on soot nucleus production in stoker-fired boilers. *Therm. Sci.* **2013**, *17*, 1317–1321. [[CrossRef](#)]
7. Demarco, R.; Consalvi, J.L.; Fuentes, A. A calibrated soot production model for ethylene inverse diffusion flames at different oxygen indexes. *Fuel* **2018**, *212*, 1–11. [[CrossRef](#)]
8. Consalvi, J.L.; Nmira, F. Transported scalar PDF modeling of oxygen-enriched turbulent jet diffusion flames: Soot production and radiative heat transfer. *Fuel* **2016**, *178*, 37–48. [[CrossRef](#)]
9. Kohse-Höinghaus, K.; Oßwald, P.; Cool, T.A.; Kasper, T.; Hansen, N.; Qi, F.; Westbrook, C.K.; Westmoreland, P.R. Biofuel combustion chemistry: From ethanol to biodiesel. *Angew. Chem. Int. Edit.* **2010**, *49*, 3572–3597. [[CrossRef](#)]
10. Esarte, C.; Abián, M.; Millera, Á.; Bilbao, R.; Alzueta, M.U. Gas and soot products formed in the pyrolysis of acetylene mixed with methanol, ethanol, isopropanol or n-butanol. *Energy* **2012**, *43*, 37–46. [[CrossRef](#)]
11. Pepiot-Desjardins, P.; Pitsch, H.; Malhotra, R.; Kirby, S.R.; Boehman, A.L. Structural group analysis for soot reduction tendency of oxygenated fuels. *Combust. Flame* **2008**, *154*, 191–205. [[CrossRef](#)]
12. Wu, J.; Song, K.H.; Litzinger, T.; Lee, S.-Y.; Santoro, R.; Linevsky, M.; Colket, M.; Liscinsky, D. Reduction of PAH and soot in premixed ethylene-air flames by addition of ethanol. *Combust. Flame* **2006**, *144*, 675–687. [[CrossRef](#)]
13. Demain, A.L. Biosolutions to the energy problem. *J. Ind. Microbiol. Biot.* **2009**, *36*, 319–332. [[CrossRef](#)] [[PubMed](#)]
14. Uyumaz, A. An experimental investigation into combustion and performance characteristics of an HCCI gasoline engine fueled with n-heptane, isopropanol and n-butanol fuel blends at different inlet air temperatures. *Energ. Convers. Manag.* **2015**, *98*, 199–207. [[CrossRef](#)]
15. Liu, H.; Ma, S.; Zhang, Z.; Zheng, Z.; Yao, M. Study of the control strategies on soot reduction under early-injection conditions on a diesel engine. *Fuel* **2015**, *139*, 472–481. [[CrossRef](#)]
16. Liu, H.; Zheng, Z.; Yao, M.; Zhang, P.; Zheng, Z.; He, B.; Qi, Y. Influence of temperature and mixture stratification on HCCI combustion using chemiluminescence images and CFD analysis. *Appl. Therm. Eng.* **2012**, *33–34*, 135–143. [[CrossRef](#)]
17. Wu, J.; Wang, H.; Zhu, L.; Hua, Y. Simulation investigation about combustion and emission characteristics of n-butanol/diesel fuel mixture on diesel engine. *Appl. Mech. Mater.* **2014**, *541*, 763–768. [[CrossRef](#)]
18. Chen, Z.; He, J.; Chen, H.; Geng, L.; Zhang, P. Comparative study on the combustion and emissions of dual-fuel common rail engines fueled with diesel/methanol, diesel/ethanol, and diesel/n-butanol. *Fuel* **2021**, *304*, 121360. [[CrossRef](#)]
19. Xu, Q.; Leathers, R.; Savage, D.; Kumar, K.; Sung, C.-J. Influence of blending n-butanol with isooctane and n-heptane on ignition delay times in a fuel ignition tester. *Energ. Fuel* **2018**, *35*, 6239–6251. [[CrossRef](#)]
20. Zheng, Z.; Yue, L.; Liu, H.; Zhu, Y.; Zhong, X.; Yao, M. Effect of two-stage injection on combustion and emissions under high EGR rate on a diesel engine by fueling blends of diesel/gasoline, diesel/n-butanol, diesel/gasoline/n-butanol and pure diesel. *Energ. Convers. Manag.* **2015**, *90*, 1–11. [[CrossRef](#)]
21. Zhang, C.; Zhang, C.; Xue, L.; Li, Y. Combustion characteristics and operation range of a RCCI combustion engine fueled with direct injection n-heptane and pipe injection n-butanol. *Energy* **2017**, *125*, 439–448. [[CrossRef](#)]
22. Yu, L.; Wu, H.; Zhao, W.; Qian, Y.; Zhu, L.; Lu, X. Experimental study on the application of n-butanol and n-butanol/kerosene blends as fuel for spark ignition aviation piston engine. *Fuel* **2021**, *304*, 121362. [[CrossRef](#)]
23. Han, J.; Wang, S.; Vittori, R.M.; Somers, L.M.T. Experimental study of the combustion and emission characteristics of oxygenated fuels on a heavy-duty diesel engine. *Fuel* **2020**, *268*, 117219. [[CrossRef](#)]
24. Ranzi, E.; Frassoldati, A.; Stagni, A.; Pelucchi, M.; Cuoci, A.; Faravelli, T. Reduced kinetic schemes of complex reaction systems: Fossil and biomass-derived transportation fuels. *Int. J. Chem. Kinet.* **2014**, *46*, 512–542. [[CrossRef](#)]

25. Sileghem, L.; Alekseev, V.A.; Vancoillie, J.; Nilsson, E.J.K.; Verhelst, S.; Konnov, A.A. Laminar burning velocities of primary reference fuels and simple alcohols. *Fuel* **2014**, *115*, 32–40. [[CrossRef](#)]
26. Fikri, M.; Herzler, J.; Starke, R.; Schulz, C.; Roth, P.; Kalghatgi, G.T. Autoignition of gasoline surrogates mixtures at intermediate temperatures and high pressures. *Combust. Flame* **2008**, *152*, 276–281. [[CrossRef](#)]
27. Saisirirat, P.; Togbé, C.; Chanchaona, S.; Foucher, F.; Mounaim-Rousselle, C.; Dagaut, P. Auto-ignition and combustion characteristics in HCCI and JSR using 1-butanol/n-heptane and ethanol/n-heptane blends. *Proc. Combust. Inst.* **2011**, *33*, 3007–3014. [[CrossRef](#)]
28. Cuoci, A.; Frassoldati, A.; Faravelli, T.; Ranzi, E. OpenSMOKE++: An object-oriented framework for the numerical modeling of reactive systems with detailed kinetic mechanisms. *Comput. Phys. Commun.* **2015**, *192*, 237–264. [[CrossRef](#)]
29. Zhao, X.; Xu, L.; Chen, C.; Chen, M.; Ying, Y.; Liu, D. Experimental and numerical study on sooting transition process in iso-octane counterflow diffusion flames: Diagnostics and combustion chemistry. *J. Energy Inst.* **2021**, *98*, 282–293. [[CrossRef](#)]
30. Westbrook, C.K.; Pitz, W.J.; Curran, H.J. Chemical kinetic modeling study of the effects of oxygenated hydrocarbons on soot emissions from diesel engines. *J. Phys. Chem. A* **2006**, *110*, 6912–6922. [[CrossRef](#)]
31. Frenklach, M.; Wang, H. Detailed modeling of soot particle nucleation and growth. *Symp. Int. Combust.* **1991**, *23*, 1559–1566. [[CrossRef](#)]
32. Wang, H.; Reitz, R.D.; Yao, M.; Yang, B.; Jiao, Q.; Qiu, L. Development of an n-heptane-n-butanol-PAH mechanism and its application for combustion and soot prediction. *Combust. Flame* **2013**, *160*, 504–519. [[CrossRef](#)]
33. Karwat, D.M.A.; Wagnon, S.W.; Wooldridge, M.S.; Westbrook, C.K. On the combustion chemistry of n-heptane and n-butanol blends. *J. Phys. Chem. A* **2012**, *116*, 12406–12421. [[CrossRef](#)] [[PubMed](#)]